Niobate nanosheet membranes with enhanced stability for nanofiltration

Nakagawa, K. ; Yamashita, H. ; Saeki, D. ; Yoshioka, T. ; Shintani, T. ; Kamio, E. ; Kreissl, H. T. ; Tsang, S. C. E. ; Sugiyama, S. ;…

(Citation)
Chemical Communications,53(56):7929-7932

(Issue Date)
2017-07-18

(Resource Type)
journal article

(Version)
Accepted Manuscript

Journal Name

COMMUNICATION

Niobate nanosheet membranes with enhanced stability for nanofiltration

Received 00th January 20xx,
Accepted 00th January 20xx

DOI: 10.1039/x0xx00000x

www.rsc.org/

K. Nakagawa,*[a] H. Yamashita,[b,c] D. Saeki,[c] T. Yoshioka,[a] T. Shintani,[a] E. Kamio,[c] H. T. Kreissl,[d] S. C. E. Tsang,[d] S. Sugiyama[b] and H. Matsuyama[c]

Niobate nanosheets are assembled into thin membranes by a vacuum filtration. The nanosheet membranes have a dense and stable structure in water via chemical cross-linking and show higher permeance and salt rejection compared with graphene oxide membranes. A water pathway model based on the void structure is presented to explain the membrane performances.

Inorganic membranes have excellent thermal, mechanical and structural strength as well as chemical resistance, and have therefore been widely studied for applications in water treatment. An ideal separation membrane for water treatment should have as thin a separation layer as possible to maximize the permeation flux, and appropriate pore sizes to ensure high rejection performance.[1] To achieve these goals, the design of new types of inorganic membranes with advanced structures is needed. Recently, two-dimensional (2D) nanosheet membranes (porous nanosheet membranes[2–6] and stacked nanosheet membranes[7–21]) have opened up a new avenue for fabricating size-selective molecular separation membranes, benefiting from their unique atomic thickness with micrometer lateral dimensions, high mechanical strength and chemical inertness. Porous nanosheet membranes consist of nanosheets with intrinsic porous structure such as in silicates[2] and zeolite[3], or drilled nanopores such as in graphene[4] for selective permeation. Although the high-quality preparation of porous nanosheets and the effective fabrication techniques of membranes should be demanded, the porous nanosheet membranes could exhibit highly molecular separation properties. Incorporating such porous nanosheets into a polymer to form mixed matrix membranes[5,6] could be alternative way for the engineering aspect. In contrast, stacked nanosheet membranes are formed by assembling nanosheets into thin membranes, and contain 2D nanochannels between the stacked sheets that allow water to pass through while rejecting unwanted solutes. The stacked nanosheet membranes could provide a more practical approach because of their separation capability using tunable 2D nanochannel.[14] Many efforts have been made to fabricate graphene-based membranes with high flux and separation performances by taking advantage of the interlayer nanochannels between sheets. However, only a narrow range of nanosheet materials, such as graphene oxide (GO)[7–16] and transition metal dichalcogenides,[17,18] have been studied for membrane preparation, although many nanosheet materials have been reported. Transition metal oxide nanosheets offer attractive surface and catalytic properties[22–24] and can also be assembled into stacked thin membranes. Therefore, they represent promising materials for potentially high-functional membranes for water separation. However, there have been few reports of metal oxide nanosheet-based membranes. Very recently, hybrid membranes consisting of GO nanosheets and titania nanosheets[19] or Co-Al (or Mg-Al) layered double hydroxide nanosheets[20] have been reported for water treatment. Nanosheet membranes consisting of only transition metal oxides, however, have not yet been demonstrated.

The structural stability of nanosheet membranes in water is another critical issue for their application, because these 2D nanosheets have a surface charge on hydration, which can cause the membrane to disintegrate via electrostatic repulsion, which results in the redispersion of the nanosheets.[21] Such membranes are unable to survive the cross-flow tests used to simulate realistic operating conditions. In practice, dead-end filtration is often utilized to evaluate the separation performance of nanosheet membranes. Stable bonding between nanosheets, as well as between nanosheets and support, are key criteria to prevent their redispersion in water.

Here, for the first time, we fabricate nanosheet membranes from single 2D molecular sheets of niobate (NbO) by a simple

[a] Center for Membrane and Film Technology, Graduate School of Science, Technology and Innovation, Kobe University, Kobe 657-8501, Japan. E-mail: knakagaw@port.kobe-u.ac.jp
[b] Department of Science and Technology, Faculty of Science and Technology, Tokushima University, Tokushima 770-8506, Japan.
[c] Center for Membrane and Film Technology, Department of Chemical Science and Engineering, Kobe University, Kobe 657-8501, Japan.
[d] Department of Chemistry, University of Oxford, Oxford, OX1 3QR, UK.
† Electronic Supplementary Information (ESI) available. See DOI: 10.1039/x0xx00000x

vacuum filtration. The stacked NbO nanosheet membranes had a dense structure and were highly stable during separation tests, even in a cross-flow membrane filtration system, because of chemical cross-linking between nanosheets. The simple method also allowed the creation of nanochannels in the stacked NbO membranes, which were found to act as high-flux nanofiltration membranes with superior rejection performances against salts.

Single-molecular layers of NbO were prepared using the hydrothermal method, with niobium(V) ethoxide ($Nb(OEt)_5$) as the niobium source in the presence of triethanolamine (TEOA) (see ESI).[23] Then, NbO nanosheets were assembled by vacuum filtration on a cellulose nitrate (CN) support modified with 3-aminopropyl-triethoxysilane (APTES). Structural analyses of the prepared samples and membranes were carried out by STEM, FE-SEM and XRD (**Figure 1**). The hydrothermal method yielded a colloidal solution, and distinct flat, single-molecular layered sheets with sharp edges were observed in the prepared sample (**Figure 1**(a)). **Figures 1**(b) and (c) show surface and cross-section SEM images of the NbO membranes prepared on a CN support modified with APTES (CN-APTES). A smooth surface is observed on the NbO membranes, while numerous pores 10–100 nm in diameter are observed on the CN and CN-APTES supports (ESI), which indicate that the surface of the supports in the NbO membrane is entirely coated with NbO nanosheets. The cross-section image (**Figure 1**(c)) shows that the thickness of the NbO membranes was about 20 nm. All of the NbO nanosheets appear to be interconnected and form a flat thin layer on the CN-APTES support. The thickness of the NbO membranes could be controlled from 20 to 90 nm by changing the volume of NbO nanosheet colloidal solution used during the vacuum filtration (ESI). **Figure 1**(e) highlights the XRD patterns of the NbO membranes with a thickness of 90 nm. In dry conditions, a broad peak at $2\theta = 8.6°$, corresponding to the (020) diffraction of stacked nanosheets with an interlayer spacing of 1.0 nm, can be clearly seen in the NbO membrane.

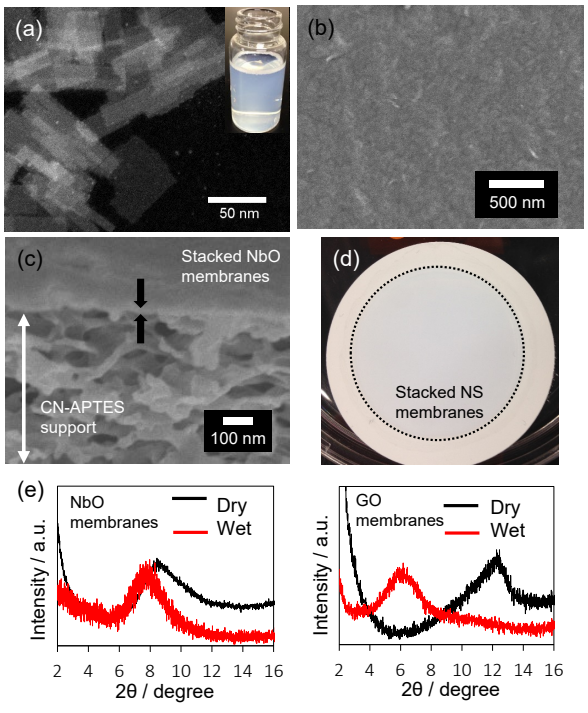

Figure 1. (a) STEM image of niobate molecular sheets, inset: Picture of niobate sheets in colloidal suspension; (b) Overview and (c) cross-section FE-SEM image of NbO membrane; (d) Pictures of NbO membranes after three-day shaking while immersed in water in a Petri dish; (e) XRD patterns of NbO membranes (left) and GO membranes (right).

Stability tests of the NbO membranes were performed by immersion in water in a Petri dish with shaking for three days. Some visible wrinkles formed on the surface of the NbO membranes prepared on the CN support, whereas the nanosheets prepared on the CN-APTES support were deposited stably (**Figure 1**(d) and Figure S6 in ESI). Hereafter, only the CN-APTES support was used for the NbO membranes. For comparison, stacked GO nanosheet membranes were also prepared by a similar vacuum filtration on a CN-APTES support (GO/CN-APTES) (ESI). The GO nanosheets were easily peeled off from the CN-APTES support after shaking in water, whereas the NbO nanosheets adhered stably to the CN-APTES support (Figure S7 in ESI). Furthermore, inspecting the structural differences in the XRD patterns between dry and wet conditions, only a slight increase of the interlayer distance from 1.0 to 1.1 nm was observed for the NbO membranes following immersion, whereas a sharper increase from 0.7 to 1.5 nm was observed for the GO membranes (**Figure 1**(e)). These results clearly indicate that the NbO membranes retain high structural stability in water. Considering that the thickness of a single NbO sheet is 0.9 nm[23] and the interlayer distance in wet condition estimated from XRD was 1.1 nm, the clearance gap between sheet layers was calculated as just 0.2 nm for the NbO membranes.

It is thus interesting to note that this vacuum filtration approach using a NbO nanosheet colloidal solution gave NbO membranes with a dense and highly stable structure in water. The source of this structural stability arises from the surface acidity of the NbO nanosheets and the roles of the amine-containing chemical binders (APTES and TEOA). Schematic diagrams of the proposed interfacial interactions in the NbO membranes are shown in Figure S8 in the ESI. First, we consider the interaction between the nanosheets and the CN-APTES support. APTES molecules are often used as a chemical binder between a support and a separation layer.[25] It is assumed that the ethoxy groups of APTES reacted with the surface hydroxyl groups of the cellulose in the CN support during the pretreatment of the support with APTES. In our previous study, NbO nanosheets behaved as very strong solid acids, possessing both Brønsted and Lewis acid sites, and thereby acted as solid acid catalysts.[24] Therefore, it appears that the amino groups of APTES reacted with the NbO nanosheets via both coordination and hydrogen bonding during the vacuum filtration and drying processes, resulting in the enhanced interaction between NbO nanosheets and CN-APTES support. Next, the interactions between nanosheet layers are considered. When the vacuum drying time was increased, the interlayer distance of the NbO membranes gradually decreased with time (ESI). These results imply that the water molecules between the stacked sheets

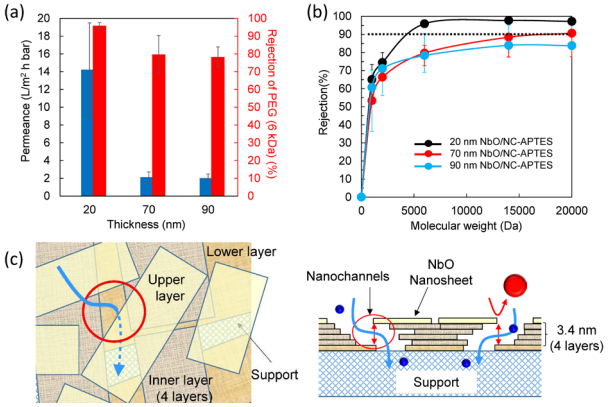

Figure 2. (a) Permeance and rejection of PEG (6 kDa) for NbO membranes with different thicknesses; (b) MWCO of PEG (dashed line) at 90% rejection for NbO membranes with different thicknesses, evaluated using PEG of various MWs; (c) Schematic diagram of nanochannels in NbO membranes (20 nm) seen from top view (left) and cross section (right).

evaporated, allowing the NbO membranes to become more tightly packed. Furthermore, XPS analysis implies the existence of TEOA in the prepared membranes (ESI). Considering these results, it appears that the amino group of TEOA directly reacted with the NbO nanosheets via coordination bonding and hydrogen bonding. Hydrogen bonding interactions between the hydroxyl groups of TEOA and those of the NbO nanosheets further strengthened the stacked nanosheet layers. Thus, the APTES and TEOA molecules effectively crosslink the sheet layers and strengthen the final membrane after vacuum drying. We believe that the facilitated formation of highly stable membranes in water using 2D NbO molecular layers is an important finding that could shed light on the rational design, assembly and more effective application of separation membranes using metal oxide nanosheets.

The membrane performances of the NbO membranes were evaluated using a cross-flow membrane filtration system. **Figure 2**(a) shows the water permeance and rejection of polyethylene glycol (PEG, Mw: 6 kDa) for NbO membranes with different thicknesses. The thinner the NbO membranes, the higher the permeances that were obtained. Rejection rates of 80–96% were achieved by all the NbO membranes, while the bare CN or CN-APTES supports without NbO layers showed extremely low rejection for 6-kDa PEG (ESI). The molecular weight cutoffs (MWCOs) of the membranes were measured using PEG samples with a range of molecular weights (**Figure 2**(b)). The results indicated that the MWCO (the Mw at which 90% rejection was achieved) decreased with decreasing thickness of the NbO membranes. For the NbO membranes with a thickness of 20 and 70 nm, the MWCOs were 4.3 and 17.0 kDa, respectively. The Stokes–Einstein radii[26] corresponding to these molecular weights can be estimated as 1.7 nm for 4.3 kDa and 3.4 nm for 17.0 kDa. Thus, from the MWCO measurements using PEG, it was concluded that nanochannels with diameters of 3.4 and 6.8 nm were formed in the NbO membranes with a thickness of 20 and 70 nm, respectively.

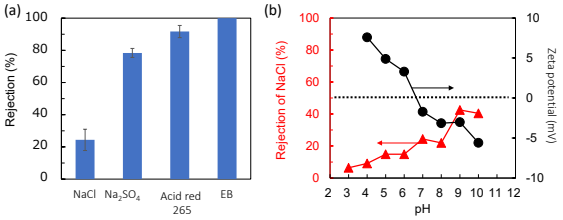

Figure 3. (a) Rejection performances of the NbO membranes (20 nm) for each salt; (b) Rejection of NaCl and zeta potential as function of pH for NbO membranes (20 nm).

In layered GO membranes,[7] water molecules permeate mainly through the interlayer nanochannels formed between the GO nanosheets, and follow a 2D path over the hydrophobic non-oxidized surface rather than the hydrophilic oxidized region. The interlayer spacing of the GO membranes increases to ~ 0.9 nm because of this hydration. It should be noted that the hydrophilic oxidized regions strongly interact with intercalating water, which may not be beneficial for water permeation.[7] Ions and molecules larger than the interlayer spacing are blocked. In our NbO membranes, the clearance gap between NbO sheets was only 0.2 nm as mentioned above, and did not substantially increase in the presence of water because TEOA acted as a chemical binder between sheets, preventing water from entering the interlayers. Thus, a suggested model of the nanochannels in the stacked NbO membranes is shown in **Figure 2**(c). When the sheets are stacked, a void structure forms as water passes through the thin membranes, resulting in the formation of nanochannels. The channels, with sizes dependent on the nanosheet thickness and numbers of layers, are created spontaneously during the vacuum filtration. The simplified schematic diagram shows void structures being formed between stacked nanosheets (**Figure 2**(c), right). In the case of NbO membranes with a thickness of 20 nm, given the value estimated from the MWCO results (3.4 nm for nanochannels), it appears that the void structures that formed by the stacking of four nanosheets (0.9 nm/sheet × 4 = 3.6 nm) became size-selective nanochannels. The possibility of size exclusion by the pores that formed between sheets in the lateral direction is evidently low, as the rejection rate did not increase with increasing nanosheet thickness. A slight decrease of PEG rejection with membrane thickness was found. An irregular stacking of nanosheets might happen by the different suction speeds or the nanosheet concentration change in the case of a high amount of nanosheet accumulation.

The rejection performances of the NbO membranes with a thickness of 20 nm were further studied using anionic dyes and salts (**Figure 3**(a)). The rejection rates of Evans blue (EB, Mw: 960.8), Acid red 265 (Mw: 635.6), Na_2SO_4 and NaCl were 99.9%, 91.7%, 78.4% and 24.4%, respectively. The surface charge (ζ-potentials) of the NbO membranes at several pH levels were measured by streaming potential measurements, and the effect on the rejection of NaCl was also investigated (**Figure 3**(b)). The ζ-potential was found to depend on pH, with an iso-electric point (IEP) of about 6.7. The NbO membranes became

negatively charged above this pH value. As the surface charge became increasingly negative, the rejection of NaCl increased. The negatively charged NbO membranes displayed a greater rejection of multivalent than monovalent anions, consistent with the Donnan exclusion mechanism.[27,28] **Tables S1 and S2** in ESI summarize a comparison of membrane performances between our NbO membranes, recently studied GO and other nanosheet membranes, and commercial nanofiltration (NF) membranes. The NbO membranes exhibited comparable performances to the commercial polymer-based NF membranes. When the performances are compared in the range of NF membranes using nanosheets, the NbO membranes exhibited superior flux and rejection of salts compared with the GO membranes prepared by a similar vacuum filtration[11,16] and comparable performances to the GO membranes prepared by an electric-field-assisted layer-by-layer assembly.[15] We attribute the high flux of the NbO membranes to the short water pathway, which results from the following two factors. First, the relatively small lateral size (around 50–200 nm) of the NbO nanosheets (**Figures 1**(a) and ESI) enables the NbO membranes to have a high aperture ratio on their top surface and a high void ratio in their interior. Second, the proposed transportation model, as shown in **Figure 2**(c), directly explains the existence of short water pathways as compared with the conventional water transportation through the interlayers of GO nanosheets (ESI). For these reasons, the NbO membranes are significantly beneficial to the water flux.

Conclusions

We fabricated NbO nanosheet membranes by a simple vacuum filtration. The NbO membranes retain structural stability in water and provide short transportation pathways for water molecules. The novel nanosheet NF membranes demonstrate higher flux and rejection of salts compared with previously reported GO NF membranes, thus fulfilling important criteria for desalination or water purification in future. This approach is also expected to be expandable to other transition metal oxide nanosheet membranes, which may open valuable perspectives for wider applications of functional membranes.

This work was supported by JSPS KAKENHI Grant Number JP16K06829 and Kurita Water and Environment Foundation Grant Number 16A078.

Notes and references

1 C. C. Striemer, T. R. Gaborski, J. L. McGrath and P. M. Fauchet, *Nature*, 2007, **445**, 749–753.
2 J. Choi and M. Tsapatsis, *J. Am. Chem. Soc.*, 2010, **132**, 448–449.
3 K. Varoon, X. Zhang, B. Elyassi, D. D. Brewer, M. Gettel, S. Kumar, J. A. Lee, S. Maheshwari, A. Mittal, C.-Y. Sung, M. Cococcioni, L. F. Francis, A. V. McCormick, K. A. Mkhoyan and M. Tsapatsis, *Science (80-.).*, 2011, **334**, 72–75.
4 S. P. Surwade, S. N. Smirnov, I. V. Vlassiouk, R. R. Unocic, G. M. Veith, S. Dai and S. M. Mahurin, *Nat. Nanotechnol.*, 2015, **10**, 459–464.
5 P. Gorgojo, D. Sieffert, C. Staudt, C. Tellez and J. Coronas, *J. Memb. Sci.*, 2012, **411**–**412**, 146–152.
6 T. Rodenas, I. Luz, G. Prieto, B. Seoane, H. Miro, A. Corma, F. Kapteijn, F. X. Llabres i Xamena and J. Gascon, *Nat. Mater.*, 2014, **14**, 48–55.
7 R. R. Nair, H. A. Wu, P. N. Jayaram, I. V. Grigorieva and A. K. Geim, *Science (80-.).*, 2012, **335**, 442–444.
8 H. Huang, Z. Song, N. Wei, L. Shi, Y. Mao, Y. Ying, L. Sun, Z. Xu and X. Peng, *Nat. Commun.*, 2013, **4**, 2979–2987.
9 H. Huang, Y. Mao, Y. Ying, Y. Liu, L. Sun and X. Peng, *Chem. Commun.*, 2013, **49**, 5963–5965.
10 M. Hu and B. Mi, *Environ. Sci. Technol.*, 2013, **47**, 3715–3723.
11 Y. Han, Z. Xu and C. Gao, *Adv. Funct. Mater.*, 2013, **23**, 3693–3700.
12 K. Huang, G. Liu, Y. Lou, Z. Dong, J. Shen and W. Jin, *Angew. Chemie - Int. Ed.*, 2014, **53**, 6929–6932.
13 R. K. Joshi, P. Carbone, F. C. Wang, V. G. Kravets, Y. Su, I. V Grigorieva, H. A. Wu, A. K. Geim and R. R. Nair, *Science (80-.).*, 2014, **343**, 752–754.
14 B. Mi, *Science (80-.).*, 2014, **343**, 740–742.
15 T. Wang, J. Lu, L. Mao and Z. Wang, *J. Memb. Sci.*, 2016, **515**, 125–133.
16 J. Wang, P. Zhang, B. Liang, Y. Liu, T. Xu, L. Wang, B. Cao and K. Pan, *ACS Appl. Mater. Interfaces*, 2016, **8**, 6211–6218.
17 L. Sun, H. Huang and X. Peng, *Chem. Commun.*, 2013, **49**, 10718–10720.
18 L. Sun, Y. Ying, H. Huang, Z. Song, Y. Mao, Z. Xu and X. Peng, *ACS Nano*, 2014, **8**, 6304–6311.
19 P. Sun, Q. Chen, X. Li, H. Liu, K. Wang, M. Zhong, J. Wei, D. Wu, R. Ma, T. Sasaki and H. Zhu, *NPG Asia Mater.*, 2015, **7**, e162.
20 P. Sun, R. Ma, W. Ma, J. Wu, K. Wang, T. Sasaki and H. Zhu, *NPG Asia Mater.*, 2016, **8**, e259.
21 C.-N. Yeh, K. Raidongia, J. Shao, Q.-H. Yang and J. Huang, *Nat. Chem.*, 2015, **7**, 166–170.
22 A. Takagaki, M. Sugisawa, D. Lu, J. N. Kondo, M. Hara, K. Domen and S. Hayashi, *J. Am. Chem. Soc.*, 2003, **125**, 5479–5485.
23 K. Nakagawa, T. Jia, W. Zheng, S. M. Fairclough, M. Katoh, S. Sugiyama and S. C. Edman Tsang, *Chem. Commun.*, 2014, **50**, 13702–13705.
24 H. T. Kreissl, K. Nakagawa, Y.-K. Peng, Y. Koito, J. Zheng and S. C. E. Tsang, *J. Catal.*, 2016, **338**, 329–339.
25 L. Bartouilh de Taillac, M. C. Porté-Durrieu, C. Labrugère, R. Bareille, J. Amédée and C. Baquey, *Compos. Sci. Technol.*, 2004, **64**, 827–837.
26 C. M. Tam and A. Y. Tremblay, *J. Memb. Sci.*, 1991, **57**, 271–287.
27 T. Tsuru, D. Hironaka, T. Yoshioka and M. Asaeda, *Sep. Purif. Technol.*, 2001, **25**, 307–314.
28 N. Hilal, H. Al-Zoubi, N. A. Darwish, A. W. Mohamma and M. Abu Arabi, *Desalination*, 2004, **170**, 281–308.

